Purinergic Signalling (2010) 6:189–200
DOI 10.1007/s11302-010-9193-8

ORIGINAL ARTICLE

Damage-induced cell–cell communication in different cochlear cell types via two distinct ATP-dependent Ca^{2+} waves

Manuela Lahne · Jonathan E. Gale

Received: 18 May 2010 / Accepted: 15 June 2010 / Published online: 6 July 2010

Abstract Intercellular Ca^{2+} waves can coordinate the action of large numbers of cells over significant distances. Recent work in many different systems has indicated that the release of ATP is fundamental for the propagation of most Ca^{2+} waves. In the organ of hearing, the cochlea, ATP release is involved in critical signalling events during tissue maturation. ATP-dependent signalling is also implicated in the normal hearing process and in sensing cochlear damage. Here, we show that two distinct Ca^{2+} waves are triggered during damage to cochlear explants. Both Ca^{2+} waves are elicited by extracellular ATP acting on P2 receptors, but they differ in their source of Ca^{2+}, their velocity, their extent of spread and the cell type through which they propagate. A slower Ca^{2+} wave (14 μm/s) communicates between Deiters' cells and is mediated by P2Y receptors and Ca^{2+} release from IP_3-sensitive stores. In contrast, a faster Ca^{2+} wave (41 μm/s) propagates through sensory hair cells and is mediated by Ca^{2+} influx from the external environment. Using inhibitors and selective agonists of P2 receptors, we suggest that the faster Ca^{2+} wave is mediated by $P2X_4$ receptors. Thus, in complex tissues, the expression of different receptors determines the propagation of distinct intercellular communication signals.

Keywords Cochlea · P2X receptors · Calcium · Damage signalling · Cell–cell signalling · ATP · Hair cells · Supporting cell

Electronic supplementary material The online version of this article (doi:10.1007/s11302-010-9193-8) contains supplementary material, which is available to authorized users.

M. Lahne · J. E. Gale (✉)
UCL Ear Institute,
University College London,
332 Gray's Inn Road,
London WC1X 8EE, UK
e-mail: j.e.gale@ucl.ac.uk

J. E. Gale
Department of Cell and Developmental Biology,
University College London,
Gower Street,
WC1E 6BT London, UK

Introduction

Cell–cell communication is essential for the normal development and function of multi-cellular organisms. One mode of cell–cell communication is via the paracrine spread of intercellular calcium (Ca^{2+}) waves. The propagation of intercellular Ca^{2+} waves involves changes in *intra*cellular Ca^{2+}, and the latter have the potential to regulate a myriad of cellular processes. In auditory hair cells, the sensory receptors of the cochlea, Ca^{2+} plays a critical role at numerous stages of sound transduction [1]. Ca^{2+} homeostasis within cochlear cells has to be tightly regulated for their optimal function and to preserve their capacity to transduce sounds. The dysregulation of intracellular Ca^{2+} is implicated in the death of most cell types [2] including hair cells [3, 4]. Hair cell death is a major cause of sensorineural hearing loss [5]. In the mammalian cochlea, hair cell loss is permanent [6], resulting in hearing impairment and deafness. Worldwide, approximately 278 million people suffer from moderate to profound hearing deficits (www.who.int/pbd/deafness/en) that affect their ability to communicate and interact socially. Despite the significant social and economic impact of this phenomenon, we know surprisingly little about the cell signalling pathways that are activated during noise and ototoxic damage and how such insults cause hair cell death.

Recent work has implicated the release of ATP in the regulation of cell–cell communication in the cochlea, both during development [7] and damage [8–10], and in both cases, ATP has been shown to trigger intercellular Ca^{2+} waves. ATP-sensitive P2 receptors are thought to sense and integrate cellular damage into downstream signalling cascades [9, 11, 12]. P2 receptors are subdivided into ionotropic P2X and metabotropic P2Y receptors that generate intracellular Ca^{2+} signals through influx of extracellular Ca^{2+} or the release from IP_3-sensitive intracellular Ca^{2+} stores, respectively [13]. In the cochlea, mechanical damage of a single hair cell triggers an increase of intracellular Ca^{2+} in surrounding cells and an intercellular Ca^{2+} wave that propagates away from the damaged area through the activation of metabotropic P2Y receptors by extracellular ATP. The wave was most prominent in the cells of the outer sulcus region [8, 14]. More recently, we showed that when a group of hair cells is damaged, an intercellular Ca^{2+} wave is clearly observed in the hair cell region. The Ca^{2+} wave contributed to the activation of extracellularly regulated kinases 1 and 2 (ERK1/2) in specific cell types within the multi-cellular tissue, i.e. Deiters' and phalangeal cells, supporting cells that neighbour the sensory hair cells [9]. The selective nature of the downstream signalling emphasises the complexity of cell–cell communication pathways in such tissue but also the necessity of research using multicellular model systems. In those experiments, the Ca^{2+} wave and its propagation through the hair cell region were not fully characterised. Here, we provide a more complete characterisation of the nature of the intercellular and intracellular Ca^{2+} signals generated as a result of mechanical damage in the cochlea. We describe two distinct intercellular Ca^{2+} waves that differ in their source of Ca^{2+}, velocities, extent of spread and also the cell types in which they occur.

Materials and methods

Solutions, dyes and drugs

The experiments were carried out in HEPES (10 mM)-buffered Hanks balanced saline solution (HB-HBSS) containing 1 mM Ca^{2+} and 1 mM Mg^{2+}. All drugs were diluted to their final concentration in HB-HBSS. In a subset of experiments, 1 mM Ca^{2+} in HB-HBSS was replaced with 1 mM Mg^{2+} and additionally chelated with 1 mM EGTA (ethylene glycol-bis(β-aminoethyl ether)-*N*,*N*,*N*′,*N*′,-tetraacetic acid). The conditions in which this external solution was used will be referred to as 0 Ca^{2+}. Stock solutions of TNP-ATP (100 mM, Tocris), ATP (100 mM) and CTP (100 mM) were prepared in 18 MΩ nanopure water. Lyophilised apyrase was reconstituted at 400 U/ml in HB-HBSS and used at a final concentration of 100 U/ml. U73122 was dissolved in DMSO at 5 mM with its final concentration being 10 μM. All stock solutions were stored at −20°C in aliquots in order to avoid freeze thawing. Ca^{2+}-sensitive dyes were purchased from Invitrogen, and all other substances unless otherwise stated were obtained from Sigma.

Isolation and culture of cochlear explants

Cochleae were isolated from neonatal Sprague–Dawley rats between P1 and P3 as described previously [9]. The procedure was carried out according to UK Animals Act of 1986 (Scientific procedures). In brief, cochlear isolation was carried out in Medium 199 with Hanks salts and 25 mM HEPES (Invitrogen, UK) supplemented with penicillin and fungizone (10 U/ml; 25 ng/ml). Cochlear basal and middle turns that had the stria vascularis and Reissner's membrane removed were cultured on Celltak®-coated (73 μg/ml; BD Biosciences, UK) MatTek® dishes (USA). Cochlear explants were cultured in Dulbecco's modified Eagle's medium with F12 (DMEM/F12, Gibco, UK) containing 5% foetal bovine serum (Gibco, UK) at 37°C in a 5% CO_2/95% air atmosphere and were used after 1 day in vitro.

Damage paradigm

Mechanical trauma was implemented using a microneedle [9]. The tip of the microneedle was positioned 15 μm above the focal plane of the hair bundle of the first row of outer hair cells (OHCs). Damage was induced by lowering the microneedle ~60 μm using the remote-controlled piezoelectric manipulator (Scientifica, UK) where it was held for 2 s and returned to its original position above the tissue.

Puff application

Nucleotides were applied locally using a micropipette picospritzer (puff application). Micropipettes (2 μm tip diameter) were pulled using a two-step electrode puller (Narashige, Japan). The micropipette was placed approximately 2 μm above the focal plane of the first row of OHCs but positioned above the outgrowing Claudius-like cells. Nucleotides were locally applied for 20 s with a pressure of 6 psi, which did not activate mechanically induced Ca^{2+} signals.

Epifluorescence Ca^{2+} imaging

Changes in the cytoplasmic Ca^{2+} concentrations were measured in cochlear cultures using the ratiometric Ca^{2+} sensitive dye 1-[6-amino-2-(5-carboxy-2-oxazolyl)-5-benzofuranyloxy]-2-(2-amino-5-methylphenoxy)ethane-*N*,*N*,*N*′,*N*′-tetraacetic acid (Fura-2). Fura-2-AM was dissolved

in 10% Pluronic®F-127 (Invitrogen) in DMSO to a 3-mM stock, and explants were loaded with 3 μM Fura-2-AM in DMEM/F12 for 40 to 50 min at 37°C in a 5% CO_2/95% air atmosphere, washed four times in HB-HBSS and left at 25°C for 20 min for the AM ester groups to be cleaved. Experiments were carried out at room temperature (20–23°C). Fura-2 was excited at 340 and 380 nm sequentially using a monochromator (Kinetic Imaging, UK), and emitted light was acquired on a 12-bit cooled CCD Sensicam camera (PCO, Germany). Illumination and image capture were controlled using IQ software (Andor Imaging, UK). Needle damage was induced after collecting baseline data for approximately 20 s. Cochlear coils were large enough to perform at least three lesions with distances of at least 500 μm separating the individual lesion sites. The first damage stimulus was always carried out in HB-HBSS containing the vehicle that the drugs were dissolved in. The second and third damage stimuli were induced following a 30-min incubation period in HB-HBSS supplemented with the drug or its vehicle. In nominally free extracellular Ca^{2+} solutions (0 Ca^{2+}), Ca^{2+} was replaced with Mg^{2+} to maintain the divalent ion concentration. During experiments, 0 Ca^{2+} solutions were exchanged 5–10 min prior to the damage stimuli (i.e. time required to establish the microneedle and imaging settings).

Fluorescence emission intensities after excitation at 340 and 380 nm were determined in 20×20 μm regions of interests (ROIs) in distinct cochlear regions using Metamorph software (Molecular Devices Inc.). ROIs were positioned at the following distances as depicted in Fig. 1d: 42–70 (56), 98–126 (112) and 154–182 (168) μm diagonally from the lesion site for the OS region; 40–60 (50), 80–100 (90) and 120–140 (130) μm to both sites from the lesion site longitudinally along the rows of HCs and at 60–80 (70), 100–120 (110) and 140–160 (150) μm horizontally from the lesion site in the Kölliker's organ (Ko) region. In the majority of experiments, the microneedle was positioned so that it was at the top of the image, which allowed 20×20 μm ROIs to be positioned from 30 up to 280 μm from the lesion site along the HC region (Fig. 2a, pre). Data were exported to Microsoft Excel and Fura-2 380/340 ratio changes were calculated after subtraction of background intensity levels. The ratio changes (ΔRs) were calculated and used to determine peak Ca^{2+} changes and Ca^{2+} wave velocities. Statistical analysis was carried out using unpaired, two-tailed Student's t tests. In addition, the U73122+0 Ca^{2+} data set was subjected to analysis of variance, and differences between groups were considered significant if $p<0.05$.

Measurement of Ca^{2+} wave velocity

The velocities of the damage-induced Ca^{2+} waves were determined along the HC region. The differential ratio (δR) signal was derived from mean ratio values by calculating interframe ratio derivative, where $\delta R=R_t-R_{t+1}$. The biggest ratio change, δR_{max}, reliably represented the onset of the calcium signal; thus, the time to δR_{max} was calculated for each ROI. ROIs were placed at different distances from the damage site, and that distance was plotted as a function of the time to δR_{max}. The data were fitted with a linear regression ($y=mx+c$) in Microsoft Excel where the slope, m, gives dx/dt, i.e. the wave velocity. This method was used to determine the velocity of the slow wave between ROIs at 60 to up to 160 μm. The speed of the faster Ca^{2+} wave and the limitation of the acquisition rate meant that there was a reduced number of time points available for curve fitting. Therefore, in this case, an 'instantaneous' velocity was calculated using $(x_{roi}-x_0)/(t_{Rmax}-t_0)$, where x_0 and t_0 are the position and onset time of the damage.

Confocal Ca^{2+} imaging

In order to assess whether HCs contribute to the Ca^{2+} wave, explants were loaded with 12 μM Oregon Green BAPTA-1-AM (OGB, stock solution, 6 mM in 10% pluronic in DMSO) and subjected to confocal microscopy. Details for loading explants with OGB were similar to Fura-2 with the exception that OGB was allowed to load for 1 h. Experiments were carried out at room temperature (20–23°C) in HB-HBSS. Confocal imaging was carried out using Zeiss 510 NLO upright or Zeiss 510 inverted confocal microscopes. OGB was excited using the 488-nm argon laser line, and emitted light passed through a 530–560-nm bandpass filter. Images were acquired at the focal plane of OHCs for the majority of experiments. Following recording of a baseline, explants were subjected to either microneedle damage or local application of ATP or CTP. Fast XZ line scan images through the thickness of the cochlear explants were acquired using a fast piezoelectric motor (PIFOC, Physik Instruments, Germany).

Results

Damage elicits the propagation of two distinct intercellular Ca^{2+} waves along the cochlear coil

Mechanical and drug-induced damage stimuli have been shown to elicit changes in intracellular Ca^{2+} concentration $[Ca^{2+}]_i$ in hair cell epithelia [3, 4, 8–10, 14, 15]. Damaging a single hair cell using a microelectrode or oscillating probe triggers an intercellular Ca^{2+} wave that propagates in an extracellular ATP-dependent fashion requiring the release of Ca^{2+} from IP_3-sensitive stores. Those studies focused primarily on the propagation of the Ca^{2+} wave from the

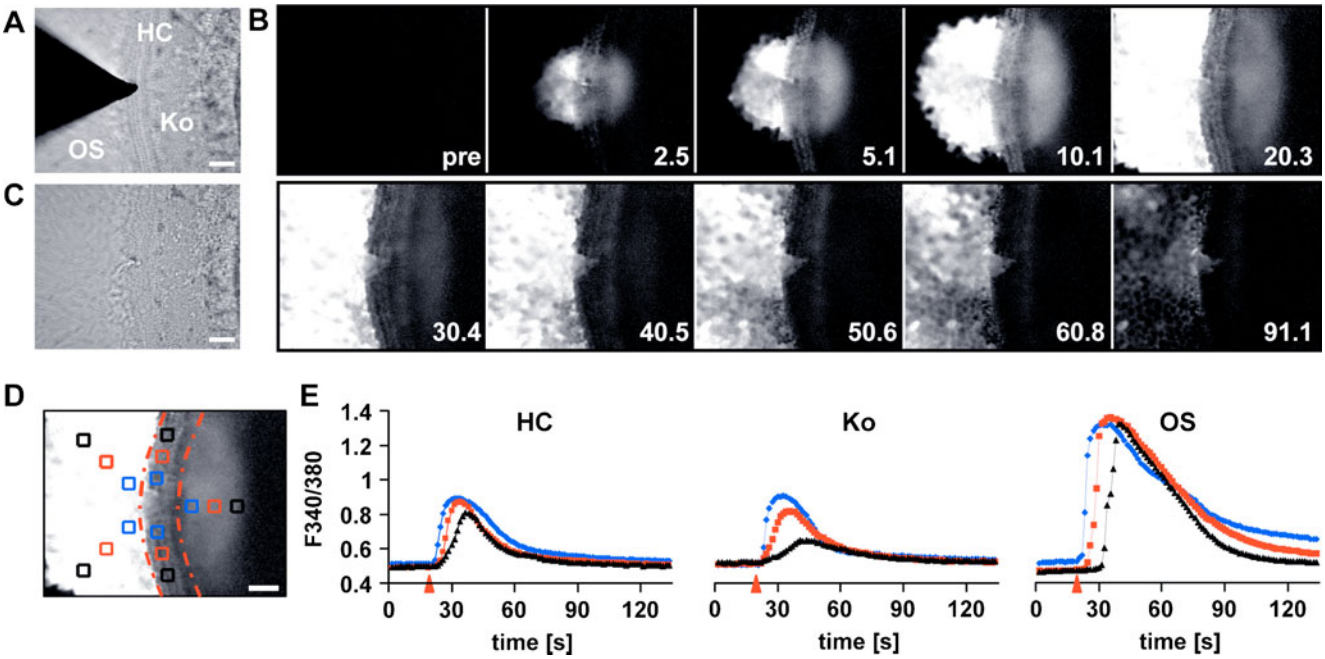

Fig. 1 Spatiotemporal properties of the cochlear damage-induced Ca^{2+} wave. **a** Brightfield image of a cochlear culture focused at the level of the stereocilial hair bundles depicting the microneedle that was used to damage the HC epithelium. The cochlear culture is comprised of HC, Ko and OS regions. **b** Series of Fura-2 ratio images (ΔR) showing the propagation of a damage-induced Ca^{2+} wave with time indicated in seconds. **c** Brightfield image of the same cochlear culture following damage. **d** Average of 15 consecutive baseline subtracted ΔR images starting at the time of damage. Regions of interest (ROIs) were placed at the following distances from the lesion site: 50 (*blue*), 90 (*red*) and 130 μm (*black*) in the HC region; 70 (*blue*), 110 (*red*) and 150 μm (*black*) in the Ko region and 56 (*blue*), 112 (*red*) and 168 μm (*black*) in the OS region. The *red lines* outline the HC region. **e** The *graphs* depict the ΔRs as a function of time for the ROIs in the HC, Ko and OS region as displayed in **d**. The *arrowheads* mark the time of damage. For the OS and HC region, the ΔRs were averaged for the two ROIs placed at the same distance from the lesion site. Scale bars, 50 μm

hair cell (HC) region into the outer sulcus (OS) region of cochlear explants, which is comprised of Hensen and Claudius-like cells. Recently, we showed that when a group of hair cells was damaged, a Ca^{2+} wave also propagated along the HC region [9]. Here, we describe the mechanisms underlying the formation and propagation of the Ca^{2+} wave in the HC region of cultured neonatal cochlear explants.

We used a microneedle to damage a small group of cells in the HC region (Fig. 1a, c) in order to study the propagation properties of the Ca^{2+} wave. Changes in $[Ca^{2+}]_i$ were monitored using the ratiometric Ca^{2+} indicator Fura-2. Propagation of the Ca^{2+} wave in all directions from the initial damage site was revealed by subtracting the baseline ratio image from the image time series (Fig. 1b). In agreement with previous reports [8–10, 14], damage triggered a rise in $[Ca^{2+}]_i$ in cells immediate to the lesion site. An intercellular Ca^{2+} wave subsequently travelled further distances into the OS region and along the HC region. In addition, the Ca^{2+} wave propagated into Kölliker's organ (Ko), part of the inner sulcus medial to the HC region in the immature rodent cochlea (Fig. 1b). Detailed spatiotemporal examination of Ca^{2+} wave propagation in the HC region revealed two temporally distinct components—in effect, two waves. The first wave spread faster with a velocity of 40.7±5.4 μm/s (n=11) and appeared to occur in a subset of cells in the HC region. A second slower wave was observed that travelled with a velocity of 13.7±0.5 μm/s (n=16), consistent with the intercellular Ca^{2+} wave described previously in the OS region [8, 14]. The faster Ca^{2+} wave was not observed in the OS or Ko region.

Subsequent recovery of $[Ca^{2+}]_i$ to baseline levels occurred within 90 s following the insult in both the HC and Ko regions (Fig. 1e). In contrast, $[Ca^{2+}]_i$ levels in the OS region did not fully recover during the time course of the recording (150 s, Fig. 1e). In order to quantify the propagation of the intercellular Ca^{2+} wave, $[Ca^{2+}]_i$ was determined in 20×20 μm ROI placed at increasing distances from the lesion site (see Fig. 1d). Figure 1e shows that in the HC and Ko region, the Ca^{2+} wave propagates to distances up to 130 and 150 μm from the lesion site, respectively. In the OS region, the Ca^{2+} wave propagated to distances greater than 168 μm from the lesion site (Fig. 1e). The magnitude of the $[Ca^{2+}]_i$ changes in the HC and Ko regions were similar, whereas those in the OS region were always significantly higher. In the HC

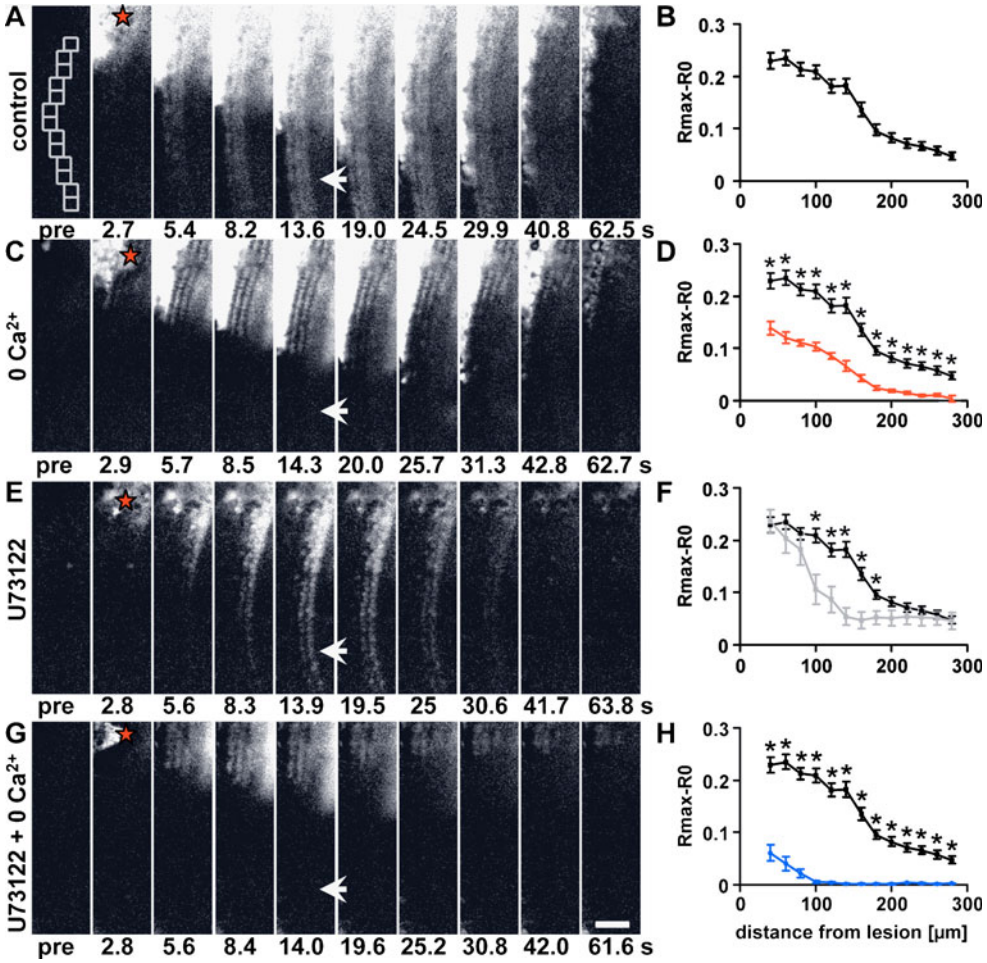

Fig. 2 Two distinct Ca^{2+} waves propagate along the HC region. **a**, **c**, **e**, **g** Time series of ΔR images showing the propagation of the damage-induced Ca^{2+} wave along the HC region in (**a**) control, (**c**) 0 Ca^{2+}, (**e**) U73122 (10 μM) and (**g**) U73122 and 0 Ca^{2+}. *Red stars* indicate the damage site, and *arrows* indicate the region of the faster Ca^{2+} wave. **b**, **d**, **f**, **h** Peak $[Ca^{2+}]_i$ changes as a function of distance from the lesion site in control (*black*, **b**, **d**, **f**, **h**), 0 Ca^{2+} (*red*, **d**), U73122 (*grey*, **f**) and U73122 and 0 Ca^{2+} (*blue*, **h**). Template in **a** (*pre*) shows the regions of interests used for quantification of peak $[Ca^{2+}]_i$ changes. Mean ± SEM, *n* (control, **a**)=22, *n* (0 Ca^{2+}, **c**)=6, *n* (U73122l, **e**)=7, *n* (U73122 and 0 Ca^{2+}, **g**)=7. Student's *t* test and analysis of variance, **p*< 0.05, Scale bar, 50 μm

and Ko regions, the Ca^{2+} waves were characterised by a decrease in the maximal $[Ca^{2+}]_i$ recorded as a function of distance (Fig. 1e).

Two sources of Ca^{2+} are required for Ca^{2+} wave propagation along the HC region

The two primary mechanisms for generation of $[Ca^{2+}]_i$ signals are the release of Ca^{2+} from intracellular stores, e.g. via the generation of IP_3, and the influx of extracellular Ca^{2+} facilitated by the opening of various types of Ca^{2+}-permeable ion channels in the plasma membrane. These Ca^{2+} sources were tested for their potential to mediate the damage-induced rise in $[Ca^{2+}]_i$ in the HC region. In order to maximise the distance over which we could assess Ca^{2+} wave propagation, we damaged hair cells at the top of the image field and monitored propagation along the HC region only. Again, we observed a faster Ca^{2+} wave that spread at least 280 μm from the lesion site (Fig. 2a) and, in many cases, appeared to propagate beyond the field of view. In contrast, the slower Ca^{2+} wave did not reach such distances. Regional analysis of the maximum change in $[Ca^{2+}]_i$ revealed a clear reduction in the signal at distances >180 μm, beyond which, the propagation was only facilitated by the faster Ca^{2+} wave (Fig. 2a, arrow, and b). When we prevented Ca^{2+} entry by removing extracellular Ca^{2+} (0 Ca^{2+}), the faster Ca^{2+} wave component was abolished (Fig. 2c). Analysis revealed that in 0 Ca^{2+}, the peak change in $[Ca^{2+}]_i$ was significantly reduced at all distances measured compared to controls (Fig. 2d). In 0 Ca^{2+}, the slower Ca^{2+} wave remained at distances <180 μm from the lesion site and, in fact, qualitative inspection of the HC region close to the damage site indicated more visible cell borders, suggesting that only one cell type participated in the formation of the Ca^{2+} wave under these conditions (compare Fig. 2a, c). When we prevented IP_3-mediated Ca^{2+} release using the phospholipase C inhibitor U73122, the peak $[Ca^{2+}]_i$ was significantly decreased only at distances between 100 and 180 μm from the lesion site (Fig. 2e, f). Again, inspection of the recorded images revealed an apparent change in the cellular response pattern in the presence of U73122, and this pattern was notably different to that observed in 0 Ca^{2+} (Fig. 2e). When 0 Ca^{2+} and U73122 were combined, propagation of the Ca^{2+} wave was reduced to less than 80 μm (Fig. 2g, h). In those combined conditions, peak $[Ca^{2+}]_i$ was significantly reduced at all distances compared to those in either 0 Ca^{2+} or U73122 alone (Supplementary Fig. 1).

Cellular localization of the fast Ca^{2+} wave

The 'salt and pepper' pattern of the cells contributing to the Ca^{2+} wave in either 0 Ca^{2+} or U73122 suggested that the faster and slower waves propagated through specific populations of cells. To test this hypothesis, we used live confocal microscopy in cochlear explants loaded with the Ca^{2+} indicator Oregon Green BAPTA-AM (Fig. 3a, c, e, g). Images acquired at the level of the OHC nuclei (see schematic illustration, Fig. 3b) confirm that damage elicited an increase in $[Ca^{2+}]_i$ in OHCs and that an intercellular Ca^{2+} wave propagated through those cells (Fig. 3c). The velocity of the Ca^{2+} wave through OHCs agreed with our estimates for the faster Ca^{2+} wave from wide-field Fura-2 data. Measurements from OHCs positioned approximately 300 μm from the centre of the damage site illustrate the kinetics of the damage-induced $[Ca^{2+}]_i$ signal (Fig. 3d). In the absence of extracellular Ca^{2+}, the damage-induced Ca^{2+} wave in OHCs was abolished (Fig. 3e, f). Upon return to control extracellular Ca^{2+} levels, the damage-induced Ca^{2+} wave observed in OHCs could be elicited again (Fig. 3g, h). Faster Ca^{2+} waves also propagate through the inner hair cells (data not shown). These data confirm that the faster Ca^{2+} wave requires extracellular Ca^{2+} and that it occurs in HCs. We infer from these data that the supporting cells are responsible for the slower IP_3-dependent Ca^{2+} wave. The opposing cell-specific patterns of the Ca^{2+} signals observed in the 0 Ca^{2+} and U73122 support this interpretation.

The distinct Ca^{2+} waves both propagate in an ATP-dependent manner

The damage-induced Ca^{2+} wave in the OS region was triggered by the release of extracellular ATP [8]. Here, we investigated whether the release of extracellular ATP was required for the propagation of the faster and slower Ca^{2+}

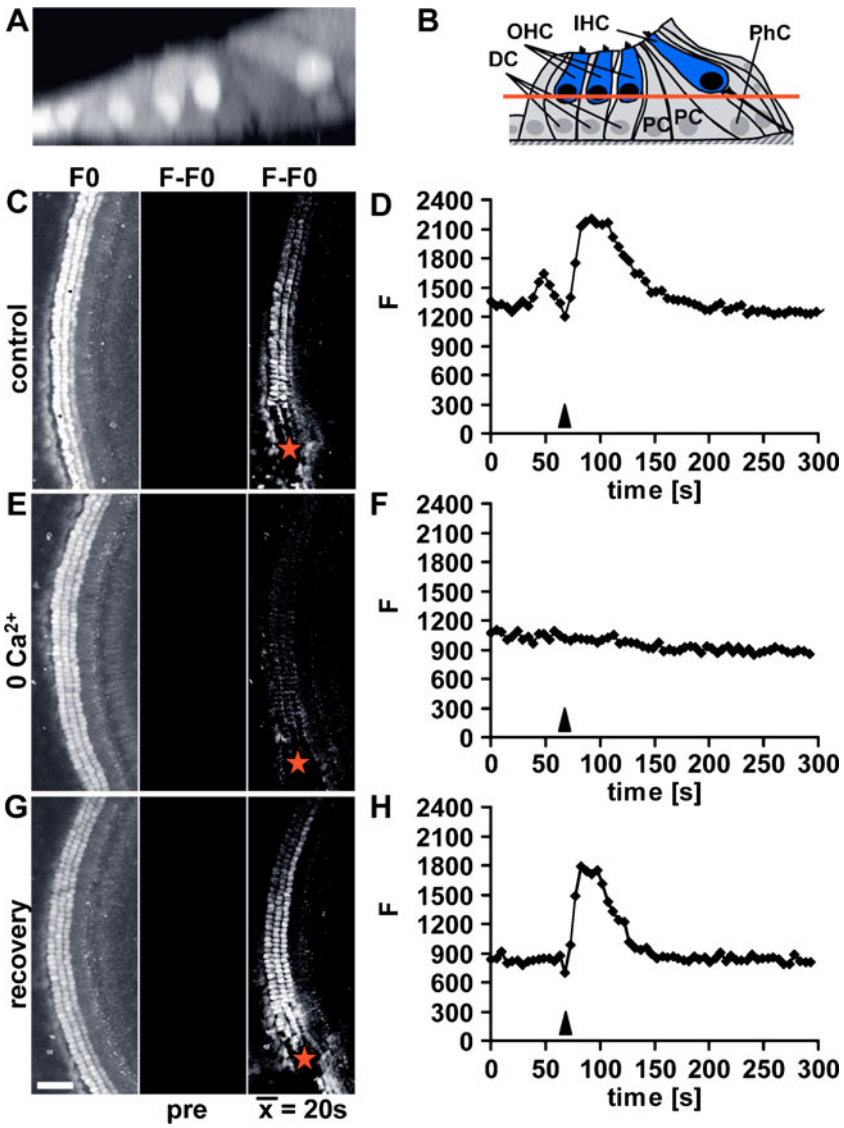

Fig. 3 Confocal imaging localises the faster Ca^{2+} wave to hair cells. **a** Confocal *x–z* projection of an Oregon Green BAPTA-AM loaded cochlear explant and (**b**) schematic cross-section of the organ of Corti illustrating its cellular composition: *OHC* outer hair cells, *IHC* inner hair cells, *DC* Deiters' cells, *PhC* phalangeal cells, *PC* pillar cells. The *red line* in **b** indicates the focal level at which confocal Ca^{2+} imaging was carried out. **c**, **e**, **g** Average of confocal images of an Oregon Green BAPTA-AM loaded cochlear explant focused at the level of the OHCs (*left column*), baseline subtracted average before the damage stimulus (*middle column*) and a time-averaged image representing the response over a period of 20 s, starting at the time of damage (*right column*). Ca^{2+} wave propagation in (**c**) control, (**e**) 0 Ca^{2+} and (**g**) following return to control medium (recovery). *Red stars* indicate the lesion site. **d**, **f**, **h** Traces depict ΔF of a single first row OHC (corresponding to **c**, **e**, **g**) in response to a microneedle-induced damage stimulus in (**d**) control, (**f**) 0 Ca^{2+} and (**h**) following return to control medium (recovery). *Arrowheads* indicate the time of damage. Images are representatives of at least three experiments. Scale bar, 50 μm

waves in the HC region. Damage was induced in cochlear explants exposed to the ATP-hydrolysing enzyme apyrase (100 U/ml). In the presence of apyrase, the damage-induced peak $[Ca^{2+}]_i$ changes were significantly decreased at all distances analysed along the HC region, indicating that both Ca^{2+} waves require the release of extracellular ATP (Fig. 4a–c).

ATP acts on purinergic P2 receptors to exert its actions. Two subtypes of P2 receptors are known: the ionotropic P2X receptors that mediate the influx of Ca^{2+} and the metabotropic P2Y receptors that initiate the release of Ca^{2+} from intracellular stores [13]. The requirement for Ca^{2+} influx and inhibition by apyrase of the faster Ca^{2+} wave seen in hair cells suggests a role for P2X receptors. In the presence of the P2X-selective antagonist TNP-ATP (100 μM), the damage-induced Ca^{2+} wave still reached distances achieved by the faster Ca^{2+} wave; the peak $[Ca^{2+}]_i$ changes were not significantly affected although a 'salt and pepper' pattern reminiscent of the effect of U73122 was observed (Fig. 4d, e). Close to the lesion site, $[Ca^{2+}]_i$ levels were decreased, albeit significantly only in a few regions (Fig. 4e). The P2X receptors that are least sensitive to TNP-ATP are $P2X_4$ and $P2X_7$ ($P2X_4$, IC_{50}=15.2 μM; $P2X_7$, IC_{50}>30 μM [16, 17]. Given the lack of effect of TNP-ATP and the lack of sensitivity of $P2X_7$ to ATP [18], we hypothesised that $P2X_4$ receptors contribute to the faster Ca^{2+} wave.

$P2X_4$ receptors are potential candidates to mediate the faster Ca^{2+} wave

Various P2 receptor subtypes have been shown to be expressed in both HCs and their surrounding supporting cells. To determine the cell specificity of P2 receptor-dependent $[Ca^{2+}]_i$ changes in cochlear explants, we locally applied ATP (for 20 s) to the HC region, and images were acquired using confocal microscopy (Fig. 5a). ATP application resulted in the increase in $[Ca^{2+}]_i$ in IHCs, OHCs and their surrounding supporting cells. Similar changes in $[Ca^{2+}]_i$ were recorded in both OHCs and IHCs (Fig. 5b). Fast line scan *x–z* images confirmed that ATP triggered changes in $[Ca^{2+}]_i$ in HCs and their surrounding supporting cells, including Deiters', Hensen's, pillar and phalangeal cells (Fig. 5a, a).

In order to test the presence of $P2X_4$ receptors in cochlear explants, we applied the agonist CTP [19]. Local application of CTP resulted in Ca^{2+} changes in OHCs and IHCs, but not in the Deiters' or pillar cells (Fig. 5c, c; d). We did observe responses to CTP in the Kolliker's cells, medial to the IHCs (M. Lahne and J.E. Gale, unpublished observations). In contrast, application of ATP was consistent in eliciting changes in $[Ca^{2+}]_i$ in all supporting cells as well as the HCs (Fig. 5aa). In the absence of extracellular Ca^{2+}, CTP did not elicit changes in $[Ca^{2+}]_i$ in hair cells confirming the ionotropic nature of the CTP response (Fig. 5e–f). As well as $P2X_4$, CTP has also been shown to act on rat $P2Y_2$ and $P2Y_4$ receptors [20]. In the present experiments, cells had been exposed to 0 Ca^{2+} for approximately 5–10 min prior to CTP application and, although unlikely, it is possible that those conditions resulted in the rundown of intracellular Ca^{2+} stores, and that this was the underlying cause for the absence of Ca^{2+} signals under such circumstances. To exclude this possibility, CTP was applied in the presence of 10 μM U73122. In the presence of U73122, OHCs and IHCs maintained their

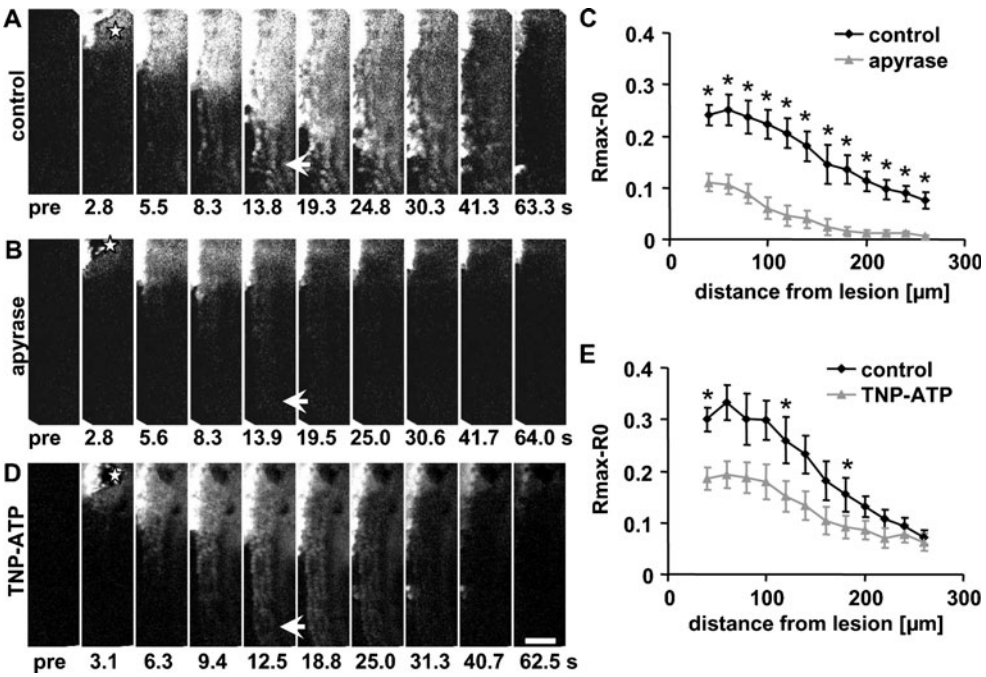

Fig. 4 ATP is a mediator of the two distinct Ca^{2+} waves in the HC region. **a**, **b**, **d** Time series of ΔR images showing the propagation of the damage-induced Ca^{2+} wave (**a**) in control, in the presence of (**b**) the ATP-degrading enzyme apyrase (100 U/ml) and (**d**) the P2X-receptor antagonist TNP-ATP (100 μM). **c**, **e** Peak $[Ca^{2+}]_i$ changes as a function of distance from the lesion site for control conditions (*black*, **c**, **e**), apyrase (*grey*, **c**) and TNP-ATP (*grey*, **e**). Mean ± SEM, *n* (control, **e**)=13, *n* (TNP-ATP, **e**)=7, *n* (control, **c**)=7, *n* (apyrase, **c**)=7, Student's *t* test, **p*<0.05. *Red stars* indicate the lesion site. Scale bar, 50 μm

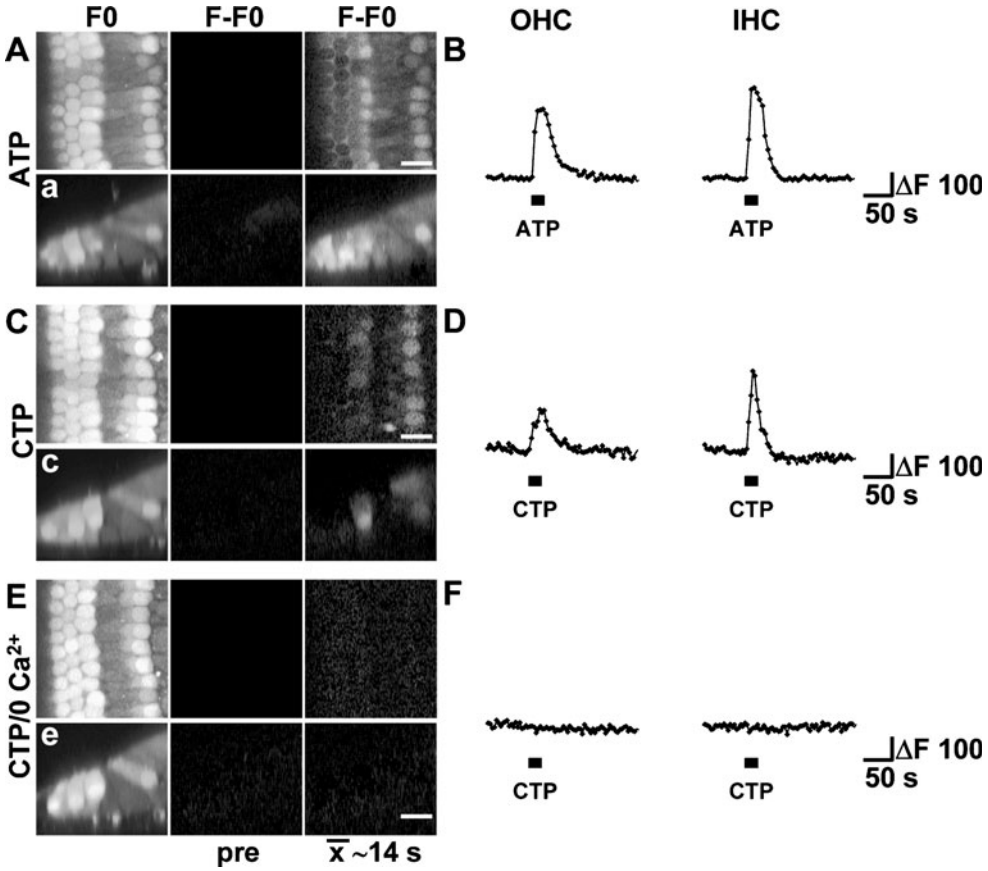

Fig. 5 $P2X_4$ receptors could mediate the faster Ca^{2+} wave. **a**, **c**, **e** Confocal images of Oregon Green BAPTA-AM loaded cochlear explants focused at the level of the HCs (*left column*), baseline subtracted time-average image representing 14 s of time prior to (*middle column*) and 14 s of time after onset of pressure application of nucleotides (*right column*). Ca^{2+} changes following pressure application of (**a**) 100 μM ATP and (**c**, **e**) 100 μM CTP in (**c**) control medium or (**e**) in 0 Ca^{2+}. *a*, *c*, *e* Confocal *x*–*z* line scan images from separate applications in the same cochlear explants exposed to the same conditions as in **a**, **c**, **e**. **b**, **d**, **f** Traces depict ΔF of a single first row OHC (*left*) and IHC (*right*, corresponding to **a**, **c**, **e**) in response to pressure application of (**b**) 100 μM ATP and (**d**) 100 μM CTP in control or (**f**) 0 Ca^{2+} conditions. Images are representatives of at least three experiments. Note that the confocal sectioning in **a**, **c, e** favours the recording of responses from the IHC and first row OHC. Scale bars, 10 μm

responsiveness to CTP, and increases in $[Ca^{2+}]_i$ were similar to those observed under control conditions (Fig. 6).

Discussion

Here, we have shown that in the neonatal cochlea, a native multi-cellular tissue, mechanical trauma triggers the release of ATP, which activates two distinct intercellular Ca^{2+} waves that propagate through two different cell types. The two waves were distinguished on the basis of (1) their extent of spread along the length of the cochlea, (2) their velocity, (3) their source of Ca^{2+} (that correlates with the underlying purinoreceptor specificity) and (4) the cell types that contribute and through which the waves propagate. The two intercellular waves have the potential to activate different downstream signals due to the differential nature of the receptors through which they operate.

Previous work in cochlear explants showed that damaging a single hair cell triggers an intercellular Ca^{2+} wave that propagated from the damage site, most obviously into the outer sulcus (OS) region [8, 14]. Here, we damaged a cluster of cells in the hair cell (HC) region with a microneedle, resulting in more significant trauma to the inner ear, such as might occur during high impulse noise [21]. Again, this triggered a rise in $[Ca^{2+}]_i$ in the cells surrounding the lesion site. However, using this larger stimulus, we made a novel observation: the propagation of two distinct Ca^{2+} waves in the HC region. Using confocal imaging, we determined that a faster wave propagated through the HCs. We showed that the faster Ca^{2+} wave reached distances of at least 280 μm and required entry of Ca^{2+} from the extracellular space. It was followed by a slower wave that spread over distances of ~180 μm and was mediated by release of Ca^{2+} from IP_3-sensitive stores. This wave propagated through supporting cells in the HC region, i.e. Deiters' and other phalangeal cells. Both the velocity and the source of Ca^{2+} that constituted the slower wave in those supporting cells were similar to that reported previously for intercellular Ca^{2+} waves measured in the OS region [8, 14]. Both waves were blocked by apyrase, indicating their dependence on the release of extracellular ATP and its subsequent activation of P2 receptors. A regenerative mechanism requiring ATP release was suggested to underlie the propagation of what we will now term the slower Ca^{2+} wave [8]. In support of a regenerative release process, the photolysis of caged IP_3 in cochlear-supporting cells did trigger ATP release, measured using a biosensor, whereas a similar effect was not observed in supporting cells from connexin 26 and 30 knockout mice,

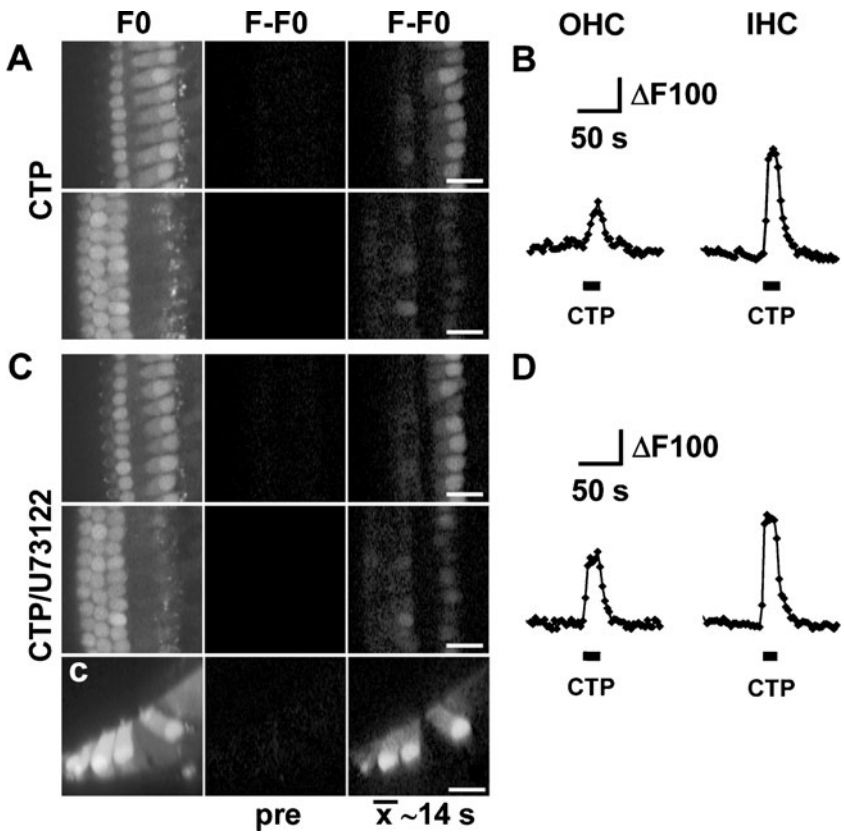

Fig. 6 CTP-induced Ca^{2+} signals in HCs are independent of IP_3-mediated Ca^{2+} release from intracellular stores. **a**, **c** Confocal images of Oregon Green BAPTA-AM loaded cochlear explants focussed at the level of the IHCs or OHCs (*left column*, *upper* or *lower row*, respectively), subtracted time-average image representing 14 s of time prior to (*middle column*) and 14 s of time after onset of pressure application of nucleotides (*right column*). $[Ca^{2+}]_i$ changes following pressure application of (**a**) 100 μM CTP in control conditions and (**c**) in the presence of U73122 (10 μM). **c** Confocal *x*–*z* line scan images obtained from the same cochlear explants as in **c** in the presence of U73122. **b**, **d** Traces depict ΔF of a single first row OHC (*left*) and IHC (*right*, corresponding to **a**, **c**) in response to pressure application of (**b**) 100 μM CTP in control or (**d**) in the presence of U73122, n=2. Scale bars, 20 μm

suggesting that connexin 26 and 30 hemichannels were required [22].

Here, propagation of the slower Ca^{2+} wave in the HC region required IP_3-sensitive stores, indicating a role for metabotropic P2Y receptors. In the OS region, propagation of the Ca^{2+} wave is mediated by UTP-sensitive P2Y receptors [14]. The similar properties of the slower Ca^{2+} waves in the OS and HC regions suggest that the same mechanism is employed. Previous functional studies have indicated the presence of P2Y receptors in Deiters' cells in guinea pigs [23, 24]. However, confirmation of the mechanism that underlies the slower waves requires a detailed description of P2Y receptor and connexin hemichannel expression and function in the cochlea.

In contrast to supporting cells, the $[Ca^{2+}]_i$ signals in HCs resulting from the faster damage-induced intercellular Ca^{2+} wave required an extracellular source of Ca^{2+}. Given the faster Ca^{2+} wave's requirement for Ca^{2+} influx and extracellular ATP, the simplest explanation is that ionotropic P2X receptors expressed by HCs were responsible. P2X receptor involvement is also consistent with the faster speed of the wave, which may well require the more rapid signal transduction process afforded by the ionotropic nature of those receptors. A number of expression and functional studies have indicated the presence of P2X receptors in HCs [25–33]. Here, we used TNP-ATP, a known P2X receptor antagonist [17], in an attempt to block the P2X-dependent faster Ca^{2+} wave. However, at 100 μM, TNP-ATP had no effect on the faster Ca^{2+} wave (most obvious, 200–260 μm from the site of damage). The P2X receptors that are sensitive to TNP-ATP are $P2X_1$, $P2X_2$, $P2X_3$, $P2X_{2/3}$, $P2X_5$ and $P2X_6$ [17, 34, 35], and those are therefore unlikely to play a role here. In contrast, $P2X_4$ and $P2X_7$ are comparatively insensitive to TNP-ATP. The ATP sensitivity of those two receptors is significantly different: $P2X_7$ receptors are only activated at relatively high ATP concentrations, EC_{50}=115 μM [18], compared to $P2X_4$ receptors, EC_{50}=5.5 μM [36]. If ATP is released and diffuses from the damage site, at distances greater than 200 μm, it is unlikely to reach the high micromolar concentrations required for $P2X_7$ receptor activation. For those reasons, we hypothesised that $P2X_4$ receptors were the most likely candidates for the receptors underlying the faster Ca^{2+} wave in HCs. The expression pattern of $P2X_4$ receptors in the intact organ of Corti has not been described, although spiral ganglion neurons are known to express this receptor subtype [37, 38]. We tested the hypothesis that HCs express functional $P2X_4$ receptors using the agonist CTP and confocal Ca^{2+} imaging. Local application of CTP elicited $[Ca^{2+}]_i$ signals in HCs that required the influx of extracellular Ca^{2+} rather than release from IP_3-sensitive stores. CTP-induced signals were not observed in supporting cells. These data indicate that HCs, but not supporting cells, express functional CTP-sensitive

P2 receptors. As well as $P2X_4$, CTP (in the 100 μM range) will activate both $P2X_2$ and $P2X_{1/5}$ receptors [35, 39, 40]. However, given their sensitivity to TNP-ATP, they are unlikely to be playing a role here [17, 35, 39, 40]. Thus, the presence of CTP-induced Ca^{2+} signals in HCs and the relative insensitivity of the faster Ca^{2+} wave in HCs to TNP-ATP are consistent with $P2X_4$ or $P2X_4$-like receptors being the mediators of the faster Ca^{2+} wave. However, interpreting the molecular nature of the native P2 receptors on the basis of pharmacological profiles determined in heterologous expression systems is not ideal. It is also likely that P2X receptors form heteromers in a native tissue such as the cochlea, and this can alter their pharmacological profiles [16, 41, 42]. Further investigation into the nature of P2 receptors and their heteromers in cochlear cells are required before we will fully understand the mechanisms underlying the damage-induced Ca^{2+} waves in the HC region.

Our data indicate that as a result of cochlear damage, extracellular ATP activates a faster most likely P2X-mediated Ca^{2+} wave in HCs and a slower P2Y-mediated Ca^{2+} wave in supporting cells (Fig. 7). The faster Ca^{2+} wave spreads to greater distances but occurs in HCs only. A question that arises is why the ATP that activates the faster wave fails to activate P2Y receptors in supporting cells at those greater distances. The ATP sensitivities of rat $P2Y_2$, $P2Y_4$ and $P2X_4$ receptors are similar (EC_{50} 2.5, 1.5 and 5.5 μM, respectively). One possible explanation for our results is that many more copies of $P2X_4$ receptors are expressed by HCs compared to the number of P2Y receptors in supporting cells. It is also possible that given the excitable nature of HCs, the ATP-induced depolarisation could activate voltage-gated Ca^{2+} channels thereby amplifying any $[Ca^{2+}]_i$ signal. Of course, these two possibilities are not mutually exclusive and would combine to enhance the sensitivity of HCs to extracellular ATP. Moreover, although $P2X_4$ receptors are relatively insensitive to TNP-ATP, at the concentration used here, we might have expected a partial reduction in $[Ca^{2+}]_i$ of the faster wave. An alternative, although less likely, explanation is that activation of P2Y receptors in HCs (possibly CTP-sensitive) could modulate the activity of a Ca^{2+}-permeable cation conductance independently from PLC activity (as our response is not inhibited by U73122). Such a response has been observed in oocytes expressing $P2Y_1$ receptors where a cation conductance was induced by adenine nucleotides independently of G-protein function [43]. However, it is not clear how rapidly this mechanism operated and whether such a mechanism would act quickly enough to enable the faster Ca^{2+} wave we describe here.

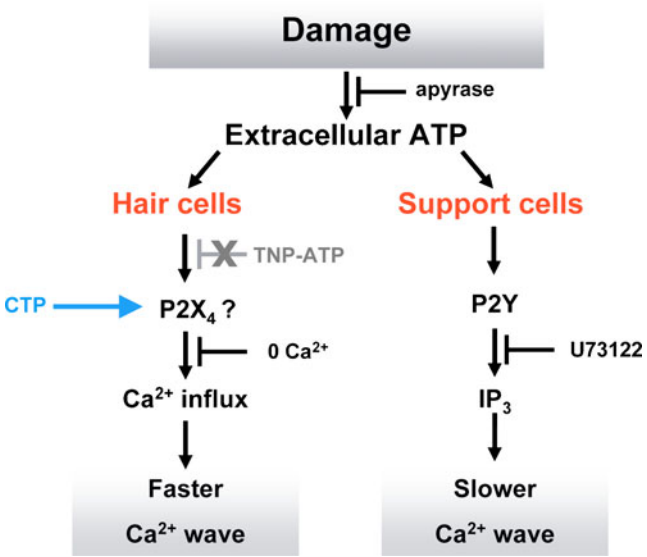

Fig. 7 A model of damage-induced Ca^{2+} wave propagation in the HC region. Acute trauma of hair cells triggers the release of ATP that induces the propagation of a faster Ca^{2+} wave in hair cells that requires Ca^{2+} influx through ion channels, most likely formed from $P2X_4$ receptors. In support cells, a slower wave is mediated by P2Y receptor activation and the subsequent release of Ca^{2+} from IP_3-sensitive stores

Our data reemphasise the general idea that in a multicellular organ such as the cochlea, one signalling molecule can exert its effect on various cell types simultaneously but in a cell-specific manner that is determined by receptor expression. Here, given the different modes of activation of the two Ca^{2+} waves, the functional consequences for the distinct cell types that are affected by those waves are also likely to differ. A vast variety of proteins including enzymes and calcium-binding proteins integrate Ca^{2+} signals into downstream signalling networks. The signalling cascade via ERK1/2 is one that can sense and integrate Ca^{2+} signals, and we have recently shown that the damage-induced Ca^{2+} wave participates in ERK1/2 activation in Deiters' and phalangeal cells [9]. One possible consequence of the damage-induced Ca^{2+} signals in HCs described herein is the activation of the protein phosphatase calcineurin, which has been implicated in noise-induced hearing loss [44]. Calcineurin, among other roles, mediates dephosphorylation of BAD, a pro-apoptotic member of the Bcl family. BAD dephosphorylation enables it to translocate from the cytoplasm to mitochondria where it promotes apoptosis [45].

In summary, we have shown that damage triggers the propagation of two distinct Ca^{2+} waves in the immature cochlea. The two Ca^{2+} waves occur in a cell type-specific manner and differ in their velocity, extent of spread, the receptors responsible for signal generation and, as a result, the source of Ca^{2+}. However, in common, both waves are mediated by the release of extracellular ATP. We confirm that P2Y receptors mediate the slower Ca^{2+} wave in supporting cells. We suggest that the primary candidate P2X receptor for the propagation of the faster Ca^{2+} wave is

the $P2X_4$ receptor subtype and provide pharmacological data in support of its expression in hair cells. Further work is required to confirm whether the damage-induced activity we describe occurs in the adult cochlea.

References

1. Mammano F, Bortolozzi M, Ortolano S, Anselmi F (2007) Ca^{2+} signaling in the inner ear. Physiol Bethesda 22:131–144
2. Bano D, Nicotera P (2007) Ca^{2+} signals and neuronal death in brain ischemia. Stroke 38(2 Suppl):674–676
3. Hirose K, Westrum LE, Stone JS, Zirpel L, Rubel EW (1999) Dynamic studies of ototoxicity in mature avian auditory epithelium. Ann NY Acad Sci 884:389–409
4. Matsui JI, Gale JE, Warchol ME (2004) Critical signaling events during the aminoglycoside-induced death of sensory hair cells in vitro. J Neurobiol 61(2):250–266
5. Nadol JB Jr (1993) Hearing loss. N Engl J Med 329(15):1092–1102
6. Chardin S, Romand R (1995) Regeneration and mammalian auditory hair cells. Science 267(5198):707–711
7. Tritsch NX, Yi E, Gale JE, Glowatzki E, Bergles DE (2007) The origin of spontaneous activity in the developing auditory system. Nature 450(7166):50–55
8. Gale JE, Piazza V, Ciubotaru CD, Mammano F (2004) A mechanism for sensing noise damage in the inner ear. Curr Biol 14(6):526–529
9. Lahne M, Gale JE (2008) Damage-induced activation of ERK1/2 in cochlear supporting cells is a hair cell death-promoting signal that depends on extracellular ATP and calcium. J Neurosci 28 (19):4918–4928
10. Mann ZF, Duchen MR, Gale JE (2009) Mitochondria modulate the spatio-temporal properties of intra- and intercellular Ca^{2+} signals in cochlear supporting cells. Cell Calcium 46(2):136–146
11. Newman EA (2001) Propagation of intercellular calcium waves in retinal astrocytes and muller cells. J Neurosci 21(7):2215–2223
12. Neary JT, Kang Y, Willoughby KA, Ellis EF (2003) Activation of extracellular signal-regulated kinase by stretch-induced injury in astrocytes involves extracellular ATP and P2 purinergic receptors. J Neurosci 23(6):2348–2356
13. King BF, Townsend-Nicholson A (2003) Nucleotide and nucleoside receptors. Tocris Rev 23
14. Piazza V, Ciubotaru CD, Gale JE, Mammano F (2007) Purinergic signalling and intercellular Ca^{2+} wave propagation in the organ of corti. Cell Calcium 41(1):77–86
15. Goodyear RJ, Gale JE, Ranatunga KM, Kros CJ, Richardson GP (2008) Aminoglycoside-induced phosphatidylserine externalization in sensory hair cells is regionally restricted, rapid, and reversible. J Neurosci 28(40):9939–9952
16. Guo C, Masin M, Qureshi OS, Murrell-Lagnado RD (2007) Evidence for functional $P2X_4/P2X_7$ heteromeric receptors. Mol Pharmacol 72(6):1447–1456
17. Virginio C, Robertson G, Surprenant A, North RA (1998) Trinitrophenyl-substituted nucleotides are potent antagonists selective for $P2X_1$, $P2X_3$, and heteromeric $P2X_{2/3}$ receptors. Mol Pharmacol 53(6):969–973
18. Surprenant A, Rassendren F, Kawashima E, North RA, Buell G (1996) The cytolytic P2Z receptor for extracellular atp identified as a P2X receptor ($P2X_7$). Science 272(5262):735–738
19. Garcia-Guzman M, Soto F, Gomez-Hernandez JM, Lund PE, Stuhmer W (1997) Characterization of recombinant human $P2X_4$ receptor reveals pharmacological differences to the rat homologue. Mol Pharmacol 51(1):109–118
20. Wildman SS, Unwin RJ, King BF (2003) Extended pharmacological profiles of rat $P2Y_2$ and rat $P2Y_4$ receptors and their sensitivity to extracellular H^+ and Zn^{2+} ions. Br J Pharmacol 140(7):1177–1186
21. Wang Y, Hirose K, Liberman MC (2002) Dynamics of noise-induced cellular injury and repair in the mouse cochlea. J Assoc Res Otolaryngol 3(3):248–268
22. Anselmi F, Hernandez VH, Crispino G, Seydel A, Ortolano S, Roper SD, Kessaris N, Richardson W, Rickheit G, Filippov MA, Monyer H, Mammano F (2008) ATP release through connexin hemichannels and gap junction transfer of second messengers propagate Ca^{2+} signals across the inner ear. Proc Natl Acad Sci USA 105(48):18770–18775
23. Dulon D, Moataz R, Mollard P (1993) Characterization of Ca^{2+} signals generated by extracellular nucleotides in supporting cells of the organ of Corti. Cell Calcium 14(3):245–254
24. Lagostena L, Mammano F (2001) Intracellular calcium dynamics and membrane conductance changes evoked by Deiters' cell purinoceptor activation in the organ of corti. Cell Calcium 29 (3):191–198
25. Mammano F, Frolenkov GI, Lagostena L, Belyantseva IA, Kurc M, Dodane V, Colavita A, Kachar B (1999) ATP-induced Ca(2+) release in cochlear outer hair cells: localization of an inositol triphosphate-gated Ca(2+) store to the base of the sensory hair bundle. J Neurosci 19(16):6918–6929
26. Ashmore JF, Ohmori H (1990) Control of intracellular calcium by ATP in isolated outer hair cells of the guinea-pig cochlea. J Physiol 428:109–131
27. Nakagawa T, Akaike N, Kimitsuki T, Komune S, Arima T (1990) ATP-induced current in isolated outer hair cells of guinea pig cochlea. J Neurophysiol 63(5):1068–1074
28. Housley GD, Kanjhan R, Raybould NP, Greenwood D, Salih SG, Jarlebark L, Burton LD, Setz VC, Cannell MB, Soeller C, Christie DL, Usami S, Matsubara A, Yoshie H, Ryan AF, Thorne PR (1999) Expression of the P2X(2) receptor subunit of the ATP-gated ion channel in the cochlea: implications for sound transduction and auditory neurotransmission. J Neurosci 19(19):8377–8388
29. Huang LC, Greenwood D, Thorne PR, Housley GD (2005) Developmental regulation of neuron-specific $P2X_3$ receptor expression in the rat cochlea. J Comp Neurol 484(2):133–143
30. Jarlebark LE, Housley GD, Raybould NP, Vlajkovic S, Thorne PR (2002) ATP-gated ion channels assembled from $P2X_2$ receptor subunits in the mouse cochlea. NeuroReport 13(15):1979–1984
31. Jarlebark LE, Housley GD, Thorne PR (2000) Immunohistochemical localization of adenosine 5′-triphosphate-gated ion channel P2X(2) receptor subunits in adult and developing rat cochlea. J Comp Neurol 421(3):289–301
32. Nikolic P, Housley GD, Luo L, Ryan AF, Thorne PR (2001) Transient expression of P2X(1) receptor subunits of ATP-gated ion channels in the developing rat cochlea. Brain Res Dev Brain Res 126(2):173–182
33. Nikolic P, Housley GD, Thorne PR (2003) Expression of the $P2X_7$ receptor subunit of the adenosine 5′-triphosphate-gated ion channel in the developing and adult rat cochlea. Audiol Neurootol 8(1):28–37
34. Jones CA, Vial C, Sellers LA, Humphrey PP, Evans RJ, Chessell IP (2004) Functional regulation of $P2X_6$ receptors by n-linked glycosylation: identification of a novel alpha beta-methylene ATP-sensitive phenotype. Mol Pharmacol 65(4):979–985
35. Wildman SS, Brown SG, Rahman M, Noel CA, Churchill L, Burnstock G, Unwin RJ, King BF (2002) Sensitization by extracellular Ca(2+) of rat P2X(5) receptor and its pharmacological properties compared with rat P2X(1). Mol Pharmacol 62(4):957–966
36. Jones CA, Chessell IP, Simon J, Barnard EA, Miller KJ, Michel AD, Humphrey PP (2000) Functional characterization of the P2X (4) receptor orthologues. Br J Pharmacol 129(2):388–394

37. Greenwood D, Jagger DJ, Huang LC, Hoya N, Thorne PR, Wildman SS, King BF, Pak K, Ryan AF, Housley GD (2007) P2X receptor signaling inhibits BDNF-mediated spiral ganglion neuron development in the neonatal rat cochlea. Development 134 (7):1407–1417
38. Xiang Z, Bo X, Burnstock G (1999) P2X receptor immunoreactivity in the rat cochlea, vestibular ganglion and cochlear nucleus. Hear Res 128(1–2):190–196
39. Haines WR, Torres GE, Voigt MM, Egan TM (1999) Properties of the novel ATP-gated ionotropic receptor composed of the P2X(1) and P2X(5) isoforms. Mol Pharmacol 56(4):720–727
40. King BF, Wildman SS, Ziganshina LE, Pintor J, Burnstock G (1997) Effects of extracellular pH on agonism and antagonism at a recombinant $P2X_2$ receptor. Br J Pharmacol 121(7):1445–1453
41. Le KT, Babinski K, Seguela P (1998) Central $P2X_4$ and $P2X_6$ channel subunits coassemble into a novel heteromeric ATP receptor. J Neurosci 18(18):7152–7159
42. Liu M, King BF, Dunn PM, Rong W, Townsend-Nicholson A, Burnstock G (2001) Coexpression of P2X(3) and P2X(2) receptor subunits in varying amounts generates heterogeneous populations of P2X receptors that evoke a spectrum of agonist responses comparable to that seen in sensory neurons. J Pharmacol Exp Ther 296(3):1043–1050
43. O'Grady SM, Elmquist E, Filtz TM, Nicholas RA, Harden TK (1996) A guanine nucleotide-independent inwardly rectifying cation permeability is associated with $P2Y_1$ receptor expression in xenopus oocytes. J Biol Chem 271(46):29080–29087
44. Minami SB, Yamashita D, Schacht J, Miller JM (2004) Calcineurin activation contributes to noise-induced hearing loss. J Neurosci Res 78(3):383–392
45. Wang HG, Pathan N, Ethell IM, Krajewski S, Yamaguchi Y, Shibasaki F, McKeon F, Bobo T, Franke TF, Reed JC (1999) Ca^{2+}-induced apoptosis through calcineurin dephosphorylation of BAD. Science 284(5412):339–343